

M ay 1995

J ulich, H L R Z 23/95

# Chiral phase transition in a lattice fermion-gauge-scalar model with $U(1)$ gauge symmetry

W .Franzki<sup>1,2,3</sup>, C .Frick<sup>1,4</sup>,  
J .Jersak<sup>1,2,5</sup> and X .Q .Luo<sup>2,6</sup>

<sup>1</sup>Institute of Theoretical Physics E, RW TH Aachen, D -52056 Aachen, Germany

<sup>2</sup>H L R Z c/o K F A J ulich, D -52425 J ulich, Germany

## Abstract

The chiral phase transition induced by a charged scalar field is investigated numerically in a lattice fermion-gauge-scalar model with  $U(1)$  gauge symmetry, proposed recently as a model for dynamical fermion mass generation. For very strong gauge coupling the transition is of second order and its scaling properties are very similar to those of the Nambu-Jona-Lasinio model. However, in the vicinity of the tricritical point at somewhat weaker coupling, where the transition changes the order, the scaling behavior is different. Therefore it is worthwhile to investigate the continuum limit of the model at this point.

Supported by Deutsches Bundesministerium für Forschung und Technologie and by Deutsche Forschungsgemeinschaft.

<sup>3</sup> E-mail address: w.franzki@kfa-juelich.de

<sup>4</sup> Present address: AM S, Querstr. 8-10, D -60322 Frankfurt a.M., Germany

<sup>5</sup> E-mail address: jersak@physik.rwth-aachen.de

<sup>6</sup> E-mail address: luo@hlrz.kfa-juelich.de

# 1 Introduction

Scalar fields are mostly introduced into the quantum field theoretical models in order to trigger some symmetry breaking already on the tree level, as in the conventional Higgs mechanism. However, fundamental scalar fields can also play an important role in a dynamical symmetry breaking occurring only beyond the perturbative expansion. An example are strongly coupled Yukawa models, which can exhibit spontaneous chiral symmetry breaking (S SB) even if the bare scalar potential in the action does not have the form of the classical Mexican hat [14].

In this paper we continue the investigation of another model of this type, the lattice chiral symmetric  $U_4$  model, considered in this context in ref. [5]. The model consists of staggered fermion field, strongly coupled gauge field  $U$  and scalar field in four dimensions (4D). The gauge symmetry is compact  $U(1)$ ,  $U(2) \times U(1)$ , and the model is confining at strong coupling. Both matter fields have unit charge and are, consequently, confined. In one phase, the Nambu phase, S SB is generated dynamically by the vectorlike interaction between the gauge field  $U$  and the fermion field, making the gauge invariant condensate  $\bar{\psi}\psi$  nonzero, in analogy to the S SB in QCD. The Goldstone bosons are composed of  $\bar{\psi}\psi$  and  $\bar{\psi}\gamma_5\psi$ .

The role of the fundamental charged scalar field is twofold. First, it shields the  $U(1)$ -charge of the fundamental fermion, so that a composite neutral physical fermion state of the form  $F = \bar{\psi}\psi$  can exist asymptotically in spite of the confinement of the  $U(1)$ -charge. In the Nambu phase its mass  $m_F$  is generated dynamically. This mechanism of fermion mass generation has been called shielded gauge mechanism in ref. [5].

Second, the scalar field has the tendency to suppress the S SB and for very strong gauge coupling induces a new second order phase transition, at which the chiral symmetry is restored and  $am_F$ , the fermion mass in lattice units, continuously approaches zero. In the scaling region of this phase transition in the Nambu phase, the model would describe a massive fermion in the continuum if it was nonperturbatively renormalizable.

We initiate the investigation of this crucial question by means of numerical simulations of the  $U_4$  model with dynamical fermions. The chiral phase transition is studied by varying suitably the gauge coupling  $\beta = 1/g^2$ , the hopping parameter  $\kappa$  and the bare fermion mass  $am_0$ . Previous studies of the present [5{13] and similar [14{19] models have indicated that the chiral phase transition, at which  $am_F$  vanishes, is smooth in some interval of strong gauge coupling, including  $\beta = 0$ . At some value  $\beta_E$  of  $\beta$  this line changes the order at the tricritical point  $E$  and continues as a first order transition line for larger  $\beta$ . We confirm these earlier results in high statistics simulations and localize with good accuracy the phase transition line and less precisely the point  $E$  ( $\beta_E \approx 0.64$ ) on it. We investigate the scaling behavior of several observables in the vicinity of the transition.

At  $\beta = 0$ , the  $U_4$  model is identical to the 4D Nambu{Jona-Lasinio (NJL) model on the lattice with the same global chiral symmetry. That model has been investigated recently in much detail [20] and its nonrenormalizability has been confirmed. We compare data obtained for  $\beta > 0$  on lattices of various sizes and at different values of the bare fermion mass  $am_0$  with those from the NJL model, using analogous analysis methods. We find that in the interval  $0 < \beta < \beta_E$ , the behavior of the  $U_4$  model is very similar to that of the NJL model.

In the close vicinity of the tricritical point  $E$  the behavior changes significantly, however. The analysis methods, that work well at smaller  $\beta$ -values, fail to describe the finite size effects and the  $am_0$ -dependence of the data. Furthermore, a new correlation length, which is of the order of the lattice spacing or less at smaller  $\beta$ -values, gets large here, indicating the presence of a new state in the spectrum of the model. This scalar bound state  $S = \bar{\psi}\psi$

has no counterpart in the NJL model.

From these observations we tentatively conclude that there are two possibilities how to approach the continuum limit of the  $U_4$  model from within the Nambu phase in such a way that the fermion mass  $m_F$  scales, and a massive fermion  $F$  is thus found in the continuum limit:

1. At some point on the chiral phase transition line at  $\beta < \beta_E$  (perhaps even at negative  $\beta$ ). Here some generalization of the NJL model is obtained, possibly similar to those discussed in ref. [21]. Either it is a nonrenormalizable theory like the NJL model itself, or a Yukawa-like model.
2. At the tricritical point  $E$ . The spectrum would contain a massive fermion  $F$ , a massive scalar  $S$  and the obligatory Goldstone bosons. It could well be that the model is renormalizable and that the shielded gauge mechanism works here, as conjectured in ref. [5]. Then the question would be, whether the resulting theory is Yukawa-like or whether some new interesting universality class exists here.

Until now we have been able to localize the tricritical point  $E$  and to analyze the properties of the chiral phase transition outside the scaling region of this point. We found that the same methods of analysis do not work in the vicinity of  $E$ . The understanding of the point  $E$  itself requires substantially more data and new analytic tools for their analysis and is beyond the scope of this work.

The outline of the paper is as follows: In the next section we define the lattice  $U_4$  model and describe its phase structure at strong gauge coupling. Here we collect the quantitative results on the position of the phase transition lines (see fig. 1). In sects. 3 and 4 we then describe in some detail the observed properties of the first order part ( $\beta_E < \beta < \beta_T$ , 0.9) and second order part ( $\beta < \beta_E$ ), respectively, of the chiral phase transition line. Our current preliminary experience with the vicinity of the point  $E$  is presented in sect. 5. Sect. 6 contains summary and outlook. In the appendix we describe another tool used in this paper in addition to the hybrid Monte Carlo method: the microcanonical fermionic averaging method developed in refs. [22,23] and extended to the  $U_4$  model [24].

## 2 Lattice $U_4$ model at strong coupling

### 2.1 The $U_4$ model

The  $U_4$  model is defined on the euclidean hypercubic lattice in 4D as follows: The staggered fermion field of charge one leads to the global  $U(1)$  chiral symmetry of the model in the chiral limit, i.e. when the bare fermion mass  $m_0$  vanishes. The gauge field link variables  $U$  are elements of the compact gauge group  $U(1)$ . The complex scalar field of charge one satisfies the constraint  $j \neq 1$ .

The action is

$$S_U = S_F + S_U + S_S; \quad (2.1)$$

where

$$S_F = \frac{1}{2} \sum_x \sum_{\mu=1}^4 \left( \bar{\psi}_x \gamma_\mu U_{x,x+\mu} \psi_{x+\mu} + \bar{\psi}_{x+\mu} \gamma_\mu U_{x+\mu,x}^\dagger \psi_x \right) + am_0 \sum_x \bar{\psi}_x \psi_x; \quad (2.2)$$

$$S_U = \sum_P \left[ \frac{1}{2} \text{Re} U_P + g |U_P|^2 \right]; \quad (2.3)$$

$$S = \sum_{x=1}^X \sum_{\mu=1}^4 U_{x,\mu} + h.c. : \quad (2.4)$$

Here  $U_p$  is the plaquette product of link variables  $U_x$ , and  $\epsilon_x = (-1)^{x_1 + \dots + x_4}$ . The hopping parameter  $\epsilon$  vanishes (is infinite) when the squared bare scalar mass is positive (negative) infinite. The bare fermion mass  $m_0$  is introduced for technical reasons, and the model is meant in the limit  $m_0 = 0$ .

## 2.2 Equivalence of the $U$ model to the four fermion theory in the strong coupling limit

At  $\epsilon = 0$ , the  $U$  model in  $d$  dimensions can be rewritten exactly as a lattice four fermion model [6]. In the path integral of the model (2.1) the scalar and gauge fields can be integrated out. This results in a purely fermionic model with the action

$$S_{4f} = \sum_{x=1}^X \sum_{\mu=1}^4 G \bar{\psi}_x \psi_{x+\mu} + \frac{1}{2} \sum_{x=1}^X \bar{\psi}_x \psi_x + \frac{am_0}{r} \sum_{x=1}^X \bar{\psi}_x \psi_x : \quad (2.5)$$

Here

$$r = r(\epsilon) = \frac{J_U}{J_1} \quad \text{and} \quad \begin{aligned} J_U &= \int_{-R}^R dU e^{2 \epsilon \text{Re} f U g U} = I_1(2 \epsilon); \\ J_1 &= \int_{-R}^R dU e^{2 \epsilon \text{Re} f U g} = I_0(2 \epsilon); \end{aligned} \quad (2.6)$$

The fermion field has been rescaled by  $\sqrt{r}$ . The parameter  $r$  is an analytic function of  $\epsilon$  increasing monotonically from  $r(0) = 0$  to  $r(1) = 1$ .

The action (2.5) obviously describes a lattice version of the NJL model. The four fermion coupling parameter  $G$  is related to  $\epsilon$  via  $r$ :

$$G = \frac{1}{4r^2} : \quad (2.7)$$

From (2.6) one sees that  $G$  is decreasing monotonically with increasing  $\epsilon$ ;  $G = 1$  at  $\epsilon = 0$ , and  $G = 0$  at  $\epsilon = 1$ .

## 2.3 Phase diagram of the $U_4$ model

The phase diagram of the  $U_4$  model with  $U(1)$  gauge symmetry obtained in this work is shown in fig. 1, and the positions of the phase transitions are listed in table 1. The used methods are described in the next sections. The phase diagram is consistent with the earlier results of unquenched simulations [10,12,13]. Qualitatively it agrees also with the quenched simulations [5,7,9]. The major difference is that the points E, T and C lie at smaller values than in the quenched case.

The chiral phase transition of the NJL model at  $\epsilon = 0$  (point N), seen in the chiral condensate and the fermion mass  $am_F$  extends to nonzero values of  $\epsilon$ . As pointed out in ref. [7], this can be derived by means of a convergent expansion around  $\epsilon = 0$ . Therefore, some properties of the NJL model have been expected to persist also at small nonzero  $\epsilon$ . We find this is so until  $\epsilon' \approx 0.55$ .

The model exhibits the Higgs phase transition (line ET and its nearly horizontal continuation to larger  $\epsilon$ ) seen in bosonic observables like plaquette and link energies. The striking feature is that, within the numerical precision, the chiral phase transition joins the Higgs

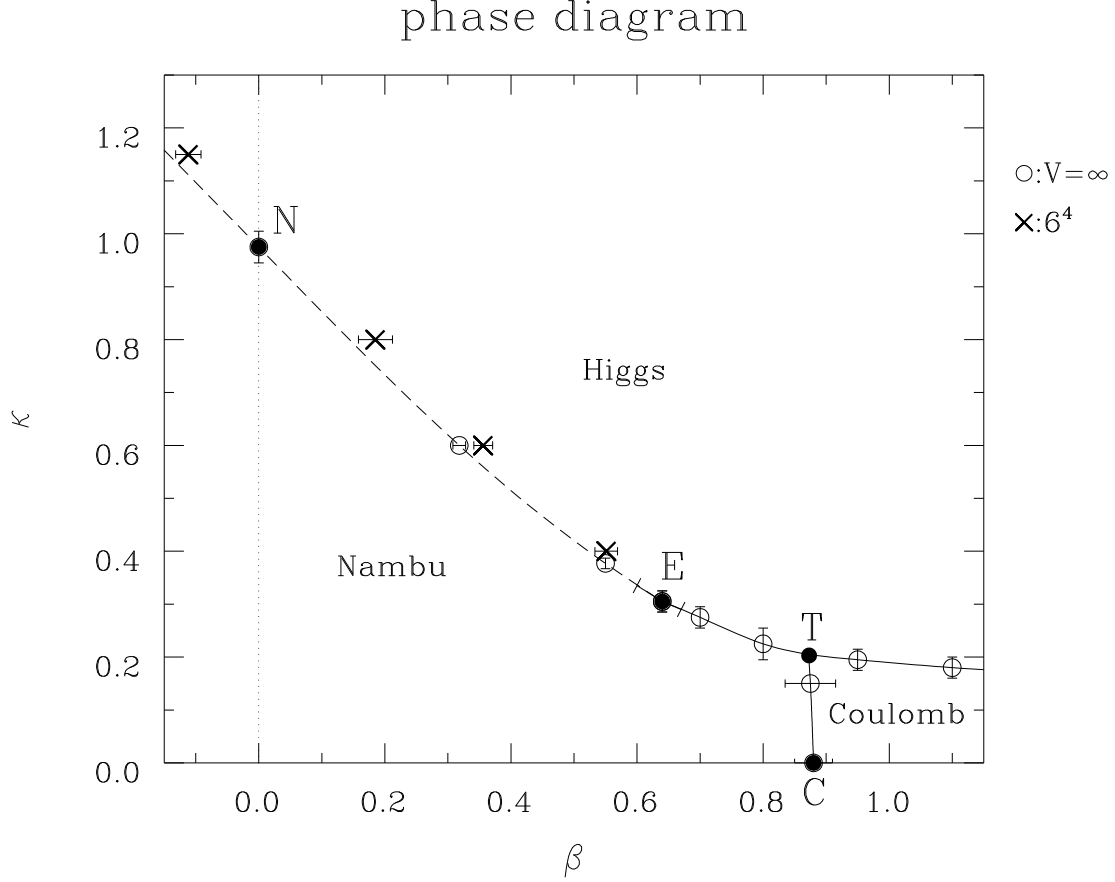


Figure 1: The phase diagram of the  $U_4$  model defined in eq. (2.1) at  $m_0 = 0$ . Three phases, the Coulomb, Higgs and Nambu phases, are found for  $\beta > 0$  and  $\kappa > 0$  or  $\kappa = 0$ . The emphasized points are:

- N : critical point of the NJL model, which is a special case of the  $U_4$  model at  $\beta = 0$ ,
- E : critical Endpoint of the Higgs phase transition line,
- T : Triple point,
- C : phase transition from the Confinement (at strong gauge coupling) to the Coulomb phase (at weak gauge coupling) in the model without the scalar field.

The dashed line corresponds to a 2<sup>nd</sup> order phase transition, full lines to 1<sup>st</sup> order transitions. The dynamical fermion mass generation takes place in the Nambu phase. A detailed discussion of this phase diagram is given in ref. [5].

The circles represent extrapolations of pseudocritical points to infinite volume and chiral limit. Also shown are the results obtained by means of the microcanonical fermionic average method on a  $6^4$ -lattice (crosses) in the chiral limit.

0.00	0.975 (30)
0.318 (10)	0.60
0.55	0.377 (10)
0.64	0.305 (20)
0.70	0.275 (20)
0.80	0.225 (30)
0.95	0.195 (20)
1.10	0.180 (20)
0.875 (40)	0.15
0.880 (30)	0.00

Table 1: Estimated position of the phase transitions in the chiral limit and on finite volume.

phase transition line ET at the tricritical point E, forming a smooth line NET. The NE and ET parts are of second and first order, respectively. To our knowledge the interweaving of the chiral and Higgs phase transition is not understood theoretically.

We concentrate on the Nambu phase, which is the area below the NET line. Here the chiral condensate  $\bar{\psi}\psi$  is nonvanishing. Both  $\phi$  and  $\psi$  fields are confined, in analogy to the quark confinement in QCD. The mass  $m_F$  of the fermion state  $F = \psi$  is nonzero, and thus the dynamical mass generation occurs.

The other phases as well as various limit cases of the phase diagram are discussed in much detail in ref. [5]. It is helpful to keep in mind that in the quenched approximation the phase diagram corresponds to that of the U(1) Higgs model (the present model without fermion field), which has been thoroughly investigated [25–28]. Even in this approximation, the chiral phase transition is observable in the chiral condensate, which is a nonlocal function of bosonic fields.

## 2.4 Definitions of observables

For a localization of the phase transition lines and a determination of the particle spectrum the following observables are used:

The normalized plaquette and link energies, defined as

$$E_P = \frac{1}{6V} \sum_P \text{Re} f U_P g; \quad (2.8)$$

$$E_L = \frac{1}{4V} \sum_{x; \mu} \text{Re} f \frac{1}{x_\mu} U_{x; \mu} g; \quad (2.9)$$

where  $V = L^3 T$  is the lattice volume. These observables are useful for the localization of the Higgs phase transition. It is convenient [28] to use the perpendicular component of these energies,  $E_\perp$ , defined as

$$E_\perp = E_L \cos \theta + E_P \sin \theta; \quad (2.10)$$

( $\theta$ ) being the slope of the chiral phase transition line at point  $(g, \phi)$ .

For the localization of the chiral phase transition line we measure the chiral condensate  $\bar{\psi}\psi$  with the stochastic estimator method.

Further we introduce the quantity

$$\chi = \frac{2}{V} \sum_{i=1}^{X=2} \frac{1}{\lambda_i} ; \quad m_0 = 0 \quad (2.11)$$

where  $\lambda_i$  are the positive eigenvalues of the massless fermion matrix. This quantity equals the chiral susceptibility in the chiral symmetric phase. Of course, in the phase with SSB it differs from the susceptibility, actually it diverges as  $O(V)$ . However, it can be rather easily calculated on small lattices by means of the microcanonical fermionic averaging method, explained in the appendix, and used for an estimate of the position of the pseudocritical point at  $m_0 = 0$ .

To calculate the mass  $m_F$  of the physical fermion we consider the gauge invariant fermionic field

$$F_x = \frac{1}{X} \sum_y \psi_x \psi_y ; \quad \bar{F}_x = \frac{1}{X} \sum_y \bar{\psi}_x \bar{\psi}_y ; \quad (2.12)$$

and determine numerically the corresponding fermion propagator in momentum space

$$G_{FAB}(p) = \frac{1}{V} \sum_{x,y} e^{i(p+A)x} F_x \bar{F}_y e^{i(p+B)y} ; \quad (2.13)$$

The  $A$ , as well as the  $B$  below, are defined in refs. [29,30]. We look for the projections

$$G(p_t) = \frac{1}{16} \text{tr} G_F(0; p_t) ; \quad G^{\parallel}(p_t) = \frac{1}{16} \text{tr} G_F(0; p_t) ; \quad (2.14)$$

which we fit by the formulas

$$G_t(p_t) = \frac{Z_F \sin p_t}{\sin^2 p_t + (am_F)^2} \quad (2.15)$$

$$G^{\parallel}(p_t) = \frac{Z_F am_F}{\sin^2 p_t + (am_F)^2} ; \quad (2.16)$$

Both fits and also those in configuration space give consistent results. The presented results are determined by means of eq. (2.15).

Further we consider the fermion-antifermion composite states, the "mesons". The time-slice operators for the mesons are given by

$$O^{ik}(t) = \sum_x S_{x,t}^{ik} \psi_x \bar{\psi}_x ; \quad (2.17)$$

with the sign factors  $S_x^{ik}$  and other details given in ref. [5]. We measure their correlation functions using point sources.

We are also interested in the scalar and the vector bosons, which are present also in the gauge-scalar model without fermions. The corresponding operators [26] are

$$O^{(S)}(t) = \frac{1}{L^3} \sum_x \text{Re} \sum_{i=1}^3 \sum_{j=1}^3 U_{x,t}^{ij} U_{x+1,t}^{ji} ; \quad (2.18)$$

$$O_i^{(V)}(t) = \frac{1}{L^3} \sum_x \text{Im} \sum_{j=1}^3 U_{x,t}^{ij} U_{x+1,t}^{ji} ; \quad i=1; 2; 3 ; \quad (2.19)$$

The masses of the scalar boson  $m_S$  and the vector boson  $m_V$  are computed from the corresponding correlation functions in momentum space. We note that the states  $S$  and  $V$  are expected to mix with the mesons carrying the same quantum numbers. In the QCD language these would be the  $\eta$  and  $\omega$  mesons, respectively.

$E_\perp$  and  $\langle \bar{\chi}\chi \rangle$   $8^4$   $am_0=0.04$  thermal cycle

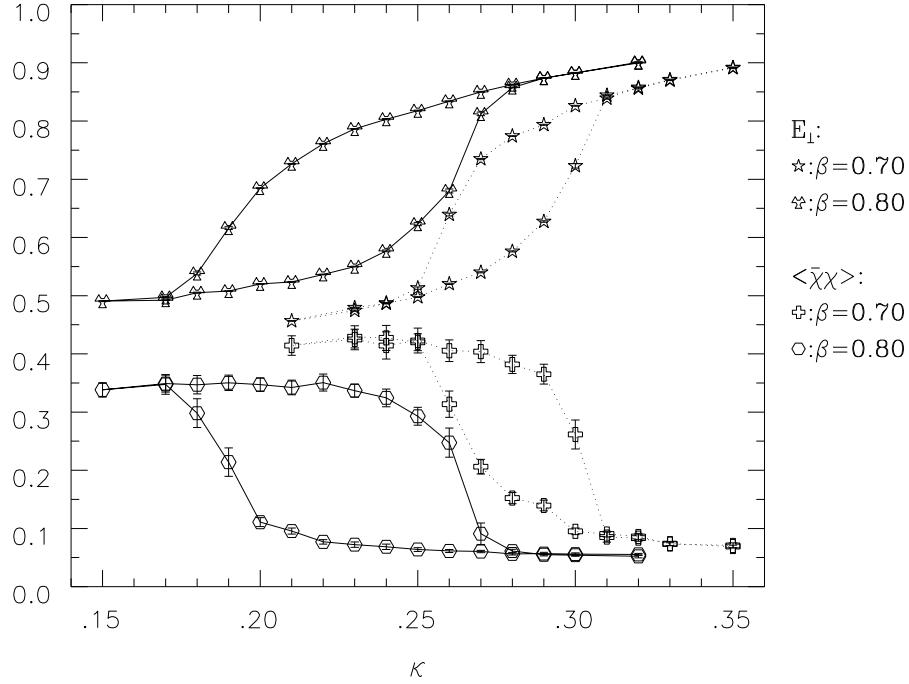


Figure 2: Thermal cycles at  $\beta = 0.70$  and  $\beta = 0.80$ . Both  $E_\perp$  and  $\langle \bar{\chi}\chi \rangle$  have hysteresees at the same place.

### 3 ET line

The ET line to the right of the point E (g. 1) is a first order phase transition line, and a continuum limit cannot be constructed here. We have investigated it mainly in order to verify the coincidence of the chiral and Higgs phase transitions. A better understanding of the ET line is also helpful for the localization and investigation of the tricritical point E.

As known from the studies of the U(1) Higgs model [25,28], the ET line (Higgs transition) is in the quenched approximation of first order in bosonic variables  $E_\perp$ ;  $am_S$  and  $am_V$ . In this approximation also the fermionic observables  $\langle \bar{\chi}\chi \rangle$  and  $am_F$  show discontinuities at the same values of the coupling parameters as the bosonic variables do. We have found similar discontinuities in the full model (i.e. with dynamical fermions) too. This is demonstrated for  $\beta = 0.70$  and  $\beta = 0.80$  on the  $8^4$  lattice for  $am_0 = 0.04$  in g. 2. Here  $E_\perp$  and  $\langle \bar{\chi}\chi \rangle$  develop hysteresees in thermal cycles in the direction with low statistics per point (100 trajectories).

The positions of the hysteresees in bosonic and fermionic observables,  $E_\perp$  and  $\langle \bar{\chi}\chi \rangle$  respectively, apparently coincide. This is so also for other values of  $am_0$  and on a  $6^4$  lattice. The hysteresees shift slightly to lower  $\kappa$ -values as  $am_0$  is decreased (by  $\approx 0.02$  between  $am_0 = 0.06$  and  $0.02$ ). Their position is quite independent of the lattice size, as usual for sufficiently strong first order phase transitions. These two observations allow us to estimate the positions of the chiral phase transition in the  $am_0 = 0$  limit (by linear extrapolation) and in finite volume (by neglecting a volume dependence). The results are indicated by two circles on the ET line in g. 1.<sup>1</sup>

To illustrate the coincidence of transitions in bosonic and fermionic observables more precisely, we show in g. 3 the observables  $E_\perp$  and  $\langle \bar{\chi}\chi \rangle$  and also  $am_F$ , all obtained in high

<sup>1</sup>The positions of the 1<sup>st</sup> order transitions to the right and below the point T in g. 1 have been determined in a similar way.



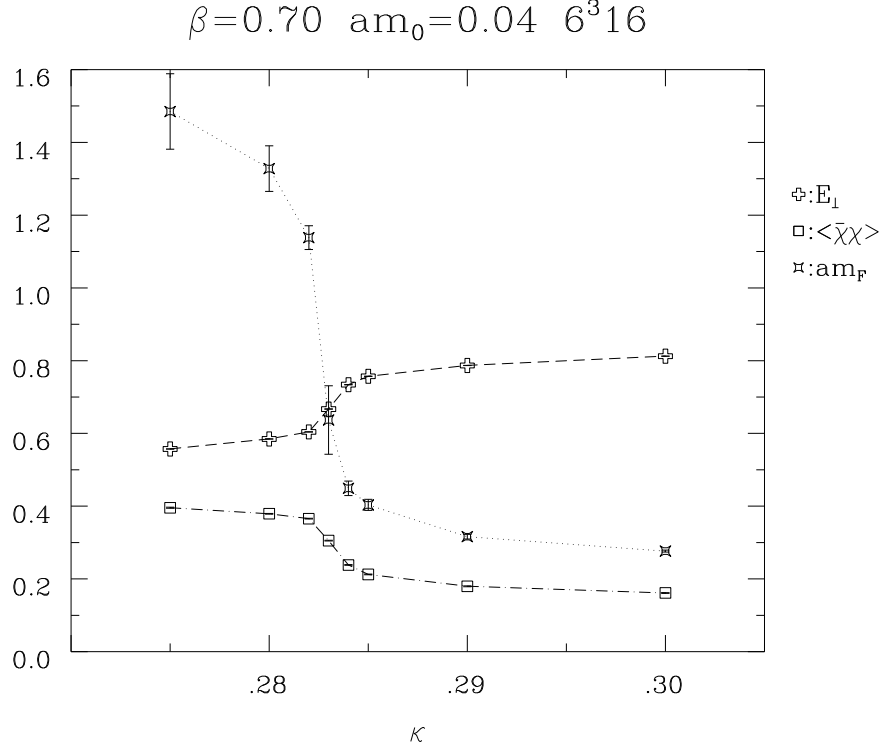


Figure 3: Energy  $E_1$  (eq. (2.10)),  $\langle \bar{\chi}\chi \rangle$  and  $am_F$  as functions of  $\kappa$  at  $\beta = 0.70$  for  $am_0 = 0.04$ . The run at  $\kappa = 0.283$  contains phase flips.

statistics runs (1600–9600 trajectories), plotted as functions of  $\kappa$  at  $\beta = 0.70$  for  $am_0 = 0.04$ . Again, the positions of the transitions agree within their accuracy on a finite lattice. At  $\kappa = 0.283$  we have observed 2–3 phase flips in  $E_1$  and  $\langle \bar{\chi}\chi \rangle$ , and the measured values of the observables are thus to some extent accidental.

In order to demonstrate that  $am_F$  has a discontinuity also in the chiral limit we have linearly extrapolated  $am_F$ , obtained in long runs, to  $am_0 = 0$  very close below and above the phase transition, as shown in fig. 4. The value of  $am_F$  at  $\beta = 0.70$  on the  $6^3 16$  lattice drops from  $\sim 1$  in the Nambu phase to nearly 0 in the Higgs phase.

The agreement of the positions of discontinuities of bosonic and fermionic observables suggests that the positions of the Higgs and chiral phase transitions on the ET line coincide. We conjecture that this is so, but we have to admit that the data leave open a logical possibility that the fermion observables do not jump exactly to zero as  $\kappa$  increases across the Higgs phase transition. The genuine chiral phase transition might take place at some larger  $\kappa$ , with small but finite values of fermionic observables in between, hidden by finite lattice size, finite  $am_0$ , etc., effects. Therefore the { very crucial } conjecture of the coincidence of both transitions should be always checked in future studies with larger resources.

## 4 NE line

The NE line is apparently of second order, as we have found no indications of metastability in the range  $0 \leq \kappa \leq 0.60$ . This was to be expected for small  $\beta$  where the chiral transition is essentially that of the NJL model [7]. As  $\beta$  increases the chiral transition gets substantially steeper, as demonstrated in fig. 5.

At  $\beta = 0$ , we have checked that our data agree within good accuracy with high precision data obtained recently [20] for the NJL model. This is not completely trivial, as we use a

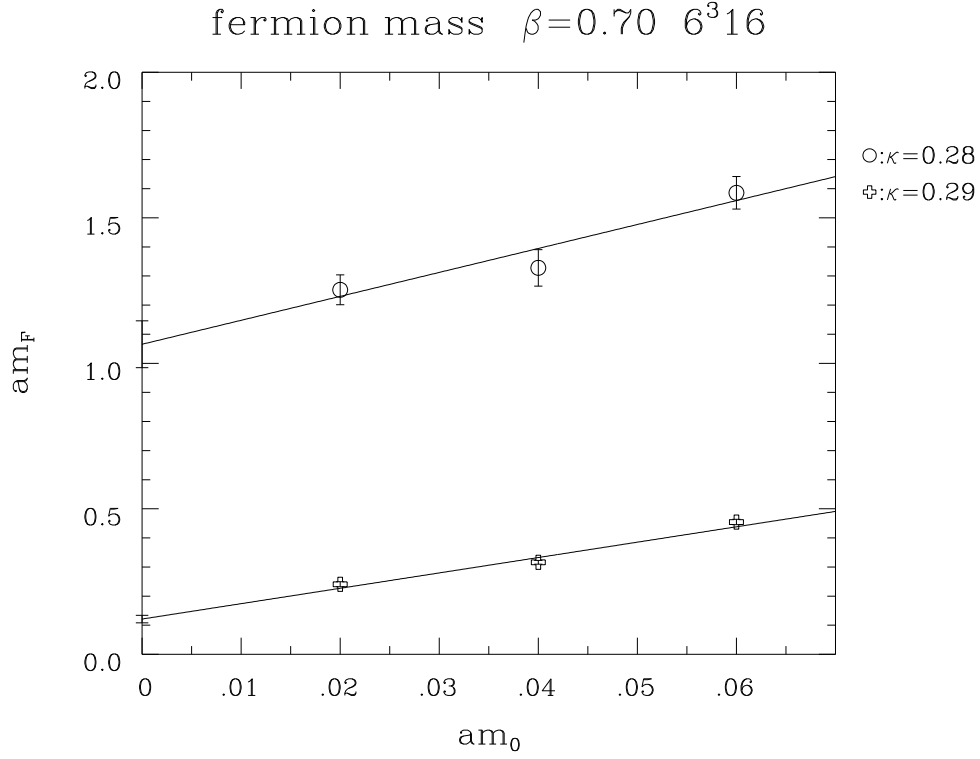


Figure 4: Fermion mass as a function of  $am_0$  at  $\beta = 0.70$  for  $\kappa = 0.28$  and  $\kappa = 0.29$  on the  $6^3 16$  lattice with a linear extrapolation to  $am_0 = 0$ .

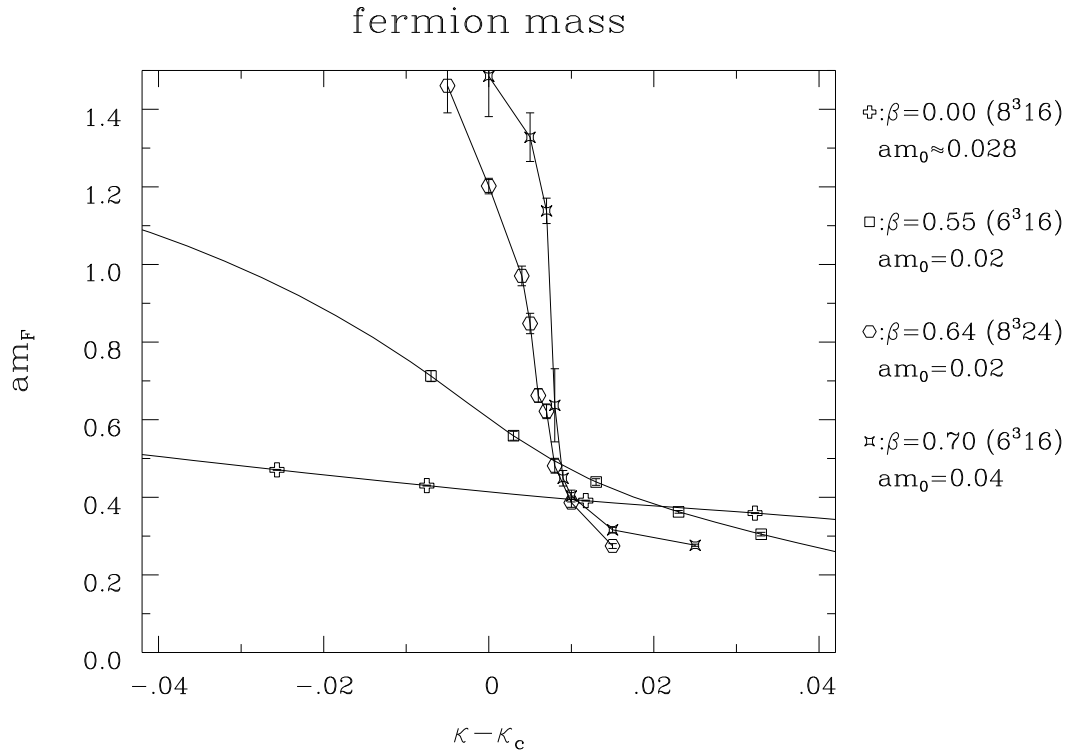


Figure 5: Comparison of the dependence of the fermion mass  $am_F$  on  $\kappa - \kappa_c$  for various  $\beta$  and  $am_0$ .  $\kappa_c$  is the extrapolated critical point at  $am_0 = 0$  in infinite volume (see table 1). The data for  $\beta = 0$  (crosses) are taken from ref. [20].

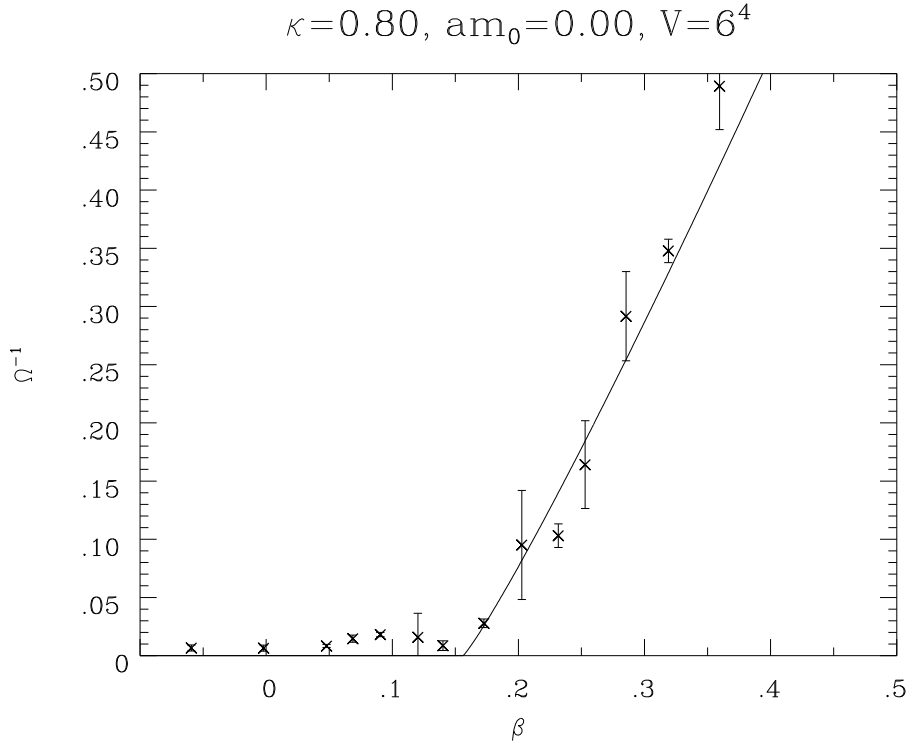


Figure 6: The observable  $Q^{-1}$  defined in eq. (2.11). The curve is a power law fit described in the text.

form of the Lee-Shrock transformation, which is different from that applied in [20] (no scalar field is used there, and the model after the transformation is not gauge invariant).

Our aim was to find out how far the critical behavior in the vicinity of the NE line is analogous to that at  $\beta = 0$ , i.e. to the NJL model, when  $\beta$  is increased. That this must be so for some finite interval in  $\beta$  around  $\beta = 0$  follows from the strong coupling expansion [7]. Our strategy is to compare our data at various  $\beta > 0$  with the data obtained in ref. [20] at  $\beta = 0$  using the same analytic Ansatz.

The position of the phase transition has been estimated on the  $6^4$  lattice using the microcanonical fermionic averaging method [24], allowing a calculation at  $am_0 = 0$ , but without an extrapolation to the infinite volume. The method is described in the appendix. The observable  $Q$ , eq. (2.11), obtained by this method at fixed  $\beta = 0.80$ , is shown in fig. 6. The positions of the pseudocritical points  $\beta_{pc}$  on  $6^4$  lattice have been determined by means of a power law fit of the form  $Q^{-1}(\beta) = A(\beta - \beta_{pc})$  to the significantly nonzero values of  $Q^{-1}$ . The obtained values of  $\beta_{pc}$  are consistent with 1 within the systematic error 0.2, estimated by fits to different sets of points. The resulting  $\beta_{pc}$  are indicated in fig. 1 by crosses.

The position  $\beta_c(\beta)$  of the chiral phase transition at  $am_0 = 0$  on the infinite volume lattice has been determined by means of the hybrid Monte Carlo algorithm at finite  $am_0$  and on various lattice sizes. The extrapolation to the infinite volume and  $m_0 = 0$  has been performed by means of a modified gap equation at  $\beta = 0, 0.55$  and at  $\beta = 0.60$  (3 circles most to the left in fig. 1) as explained below. The results of the extrapolation are listed in table 1.

The modified gap equation has been used in ref. [20] for analytic description of the data for the chiral condensate in the NJL model on different lattices and for different  $am_0$ . It is defined as follows:

$$h^{-1}_i = \frac{1}{V} \sum_k \frac{p^J}{J^2 + c_1^2 \sin^2 k} \quad (4.1)$$

with

$$J = c_1^2 w(\beta; \kappa) h^{-1} + c_2 am_0 : \quad (4.2)$$

This equation is a generalization of the usual gap equation by introducing free parameters  $w(\beta; \kappa)$ ,  $c_1$  and  $c_2$  independent of  $am_0$  and lattice size. The  $c_1$  and  $c_2$  are expected to be nearly independent of  $\beta$  for  $\beta' \ll \beta_c$ . In the original gap equation for the NJL model their values are  $w(\beta; 0) = 8G(\beta)$ ,  $c_1 = r(\beta)$  and  $c_2 = 1$  (for the definition of  $G$  and  $r$  see eq. (2.6) and (2.7)). For  $\beta' \ll \beta_c$  the variation of  $r(\beta)$  is small at  $\beta = 0$ . To use the modified equation also for  $\beta' > 0$  we neglect this presumably weak dependence and keep  $c_1$  constant. Up to this simplification and some redefinitions of the parameters the equation (4.1) is the same as eq. (3.4) of ref. [20]. We can thus compare our data analysis at  $\beta' > 0$  with that performed in [20] at  $\beta' = 0$ .

We have used eq. (4.1) as an implicit equation for  $w$ . For each value of  $\beta$  we choose  $c_1$  and  $c_2$ , and then for each  $\beta' \ll \beta_c$ ,  $am_0$  and lattice size we determine  $w$  from the value of  $h^{-1}$ . The choice of  $c_1$  and  $c_2$ , independent of  $\beta$ ,  $am_0$  and lattice size, is made so that  $w$  is at fixed  $\beta$  independent of  $am_0$  and lattice size as much as possible. We minimize the expression

$$\sum_i (w_i - \bar{w}(\beta; c_1; c_2))^2 \frac{1}{\delta_i^2} \quad (4.3)$$

with respect to variations of  $c_1$  and  $c_2$ . Here  $w_i$  and  $\delta_i$  are, respectively, values and errors of  $w$  obtained by means of (4.1) from  $h^{-1}$  value and its statistical error at different data points  $i$ .  $\bar{w}$  is the average of  $w_i$  for the same  $\beta$ ,  $c_1$  and  $c_2$ .

The possibility of choosing  $c_1$  and  $c_2$  in such a way that  $w$  depends only on  $\beta$  means that the modified gap equation is applicable at this  $\beta$ . The results for  $w(\beta)$  are shown in fig. 7a,b. If the modified gap equation works, it can be used for an extrapolation to chiral limit and infinite volume, and the critical value  $w_c$  of  $w$ , below which  $h^{-1}$  vanishes (see fig. 7), is obtained. The critical point  $\beta_c(\kappa)$  at the given  $\kappa$  is then determined from  $w(\beta_c) = w_c$ .

As seen from fig. 7a and 7b, the modified gap equation describes in the above sense the data very well at  $\beta = 0$  and  $\beta = 0.55$  for various  $am_0$  and different lattice sizes. The agreement at  $\beta = 0.55$  (fig. 8) is nearly as good as at  $\beta = 0$ , cf. ref. [20]. The constants  $c_1$  and  $c_2$  have nearly the same values for these two  $\beta$  values. Therefore this method can be used also for fixed and varying  $\beta' \ll \beta_c$ . We have done this at  $\beta = 0.60$ . The lowest curve in fig. 8 describes the extrapolation to infinite volume and  $am_0 = 0$ . In this way the position  $\beta_c(\kappa)$  of the chiral transition has been obtained for 3 points on the NE line.

In this way one can obtain also pseudocritical points on lattices of finite size, again by determining values of  $w$  for which  $h^{-1}$  vanishes. The corresponding  $\beta_{pc}$  on the  $6^4$  lattice are consistent with those obtained by the microcanonical fermion average method.

Another way to investigate the scaling properties of the NJL model in [20] was to plot  $h^{-1/2}$  as a function of  $am_0 = h^{-1}$  (Fisher plot). This is motivated by the general scaling relation

$$am_0 = b_1 (\beta - \beta_c) h^{-1/\nu} + b_2 h^{-1} ; \quad (4.4)$$

where the mean field values of the exponents,  $\nu = 3$  and  $\beta_c = \frac{1}{2}$ , are assumed. Provided these values are correct, the data for a fixed  $\kappa$  on a given lattice should form straight lines. As seen in fig. 9a, for  $\beta = 0.55$  the mean field exponents describe the data quite well. We again find a large similarity between our data at  $\beta = 0.55$  and the data at  $\beta = 0$  in ref. [20]. This includes also the observed finite size effect.

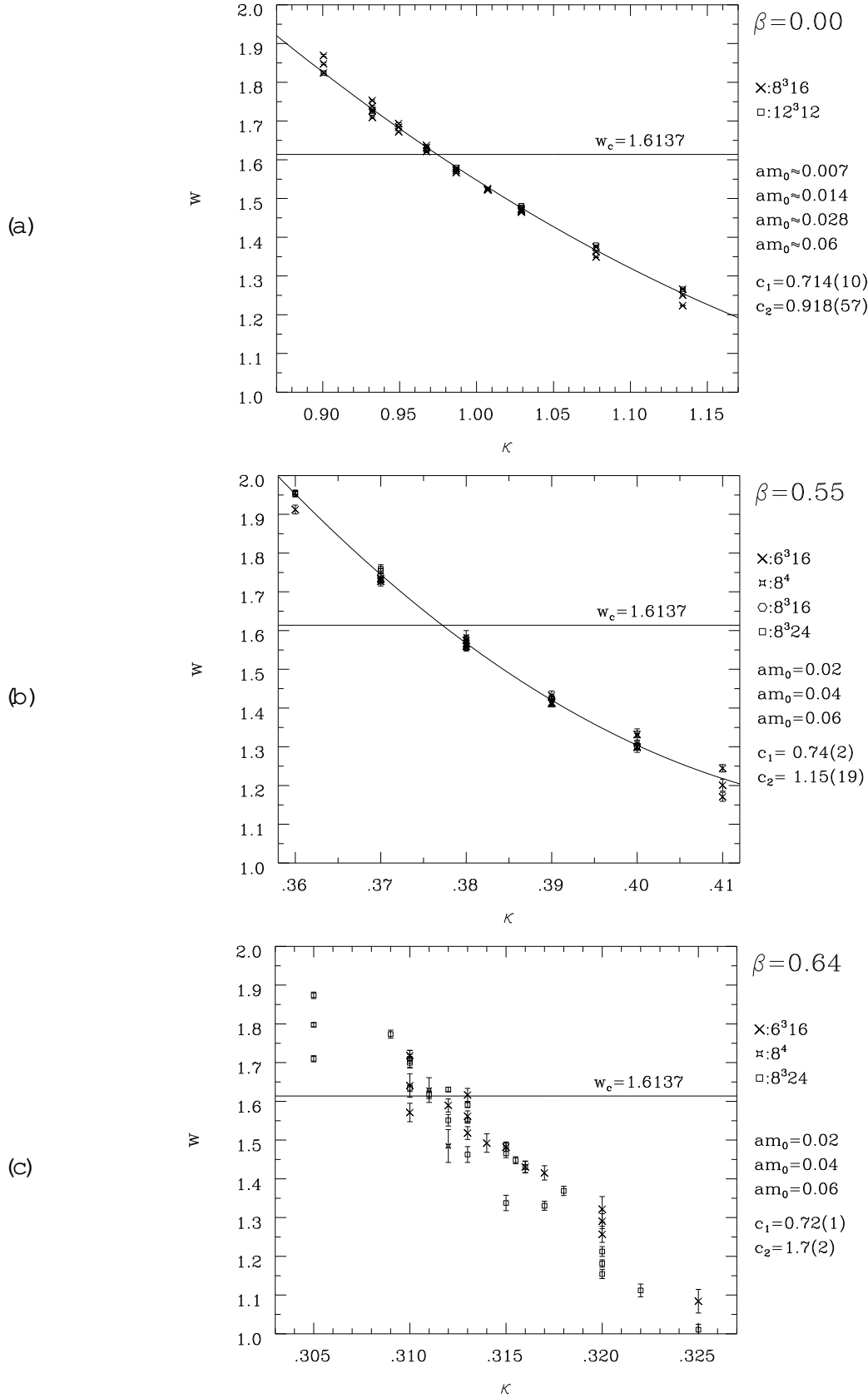


Figure 7: The parameter  $w$  in the modified gap equation as a function of  $\kappa$  for (a)  $\beta = 0$  (NJL model), (b)  $\beta = 0.55$  and (c)  $\beta = 0.64$ . For  $\beta = 0$  and  $\beta = 0.55$   $w$  is independent of lattice sizes and bare mass and the modified gap equation describes the data well. For  $\beta = 0.64$ , which is close to the point E, this is no longer so. The curves in (a) and (b) are quadratic function fits to the  $w$ -values. The data in figure (a) are taken from ref. [20].

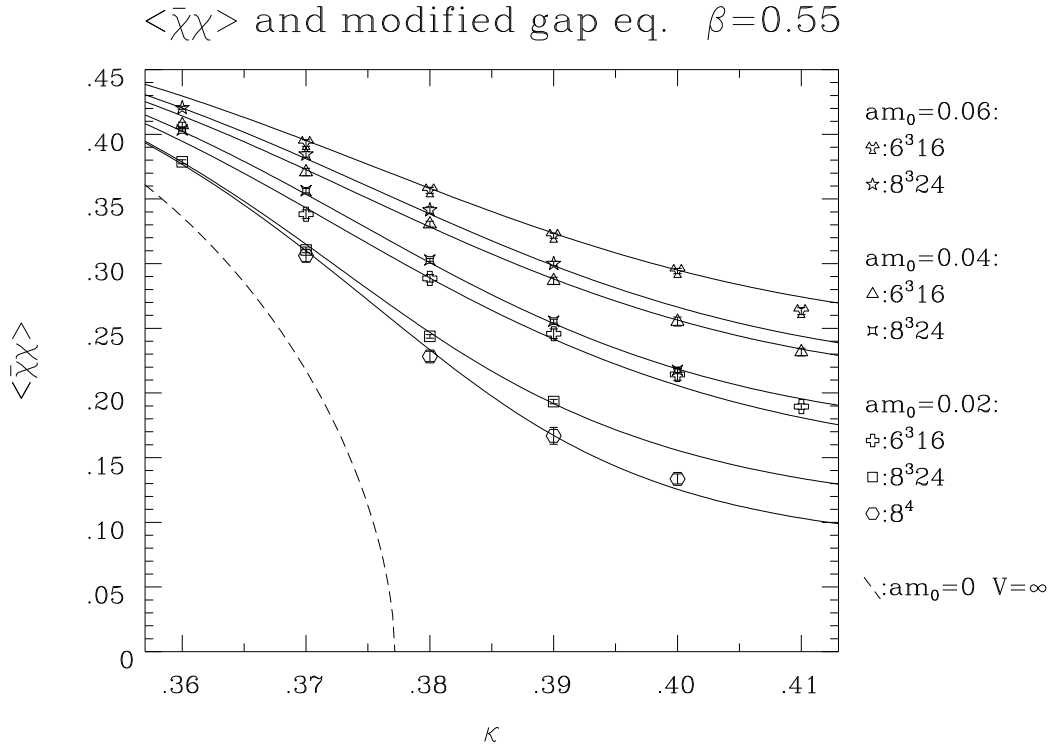


Figure 8: Comparison of the modified gap equation and the data at  $\beta = 0.55$ . The parameter  $w$  depends on  $K$  as described by the line in Fig. 7b, whereas the parameters  $c_1$  and  $c_2$  are fixed at values  $c_1 = 0.74$  and  $c_2 = 1.1$ . The extrapolation to infinite volume and  $am_0 = 0$  is represented by the dashed line.

## 5 Vicinity of the point E

It is notoriously difficult to localize a tricritical point. Our best current estimate is  $\beta_E = 0.64^{+0.03}_{-0.04}$  and  $K_E = 0.305^{+0.03}_{-0.015}$  (point E in Fig. 1). It is based on the extrapolation in  $\beta$  of latent heat to zero and on the localization of minimum of scalar mass  $am_s$  as described below. Finite size effects are only roughly taken into account.

We have tried to apply at  $\beta = 0.64$  the same method of analysis to the scaling behavior as at  $\beta = 0$  and  $\beta = 0.55$ . It turns out that both above methods do not work anymore. The modified gap equation does not describe the data if  $w$  should depend only on  $K$  and not on  $am_0$  and lattice size. This is seen in Fig. 7c. Here we show the values of  $w$  obtained for such a set of parameters  $c_1$  and  $c_2$ , for which the dependence of  $w$  on  $am_0$  and lattice size is minimal. Also the test for mean field values of exponents  $\nu$  and  $\beta$  by means of the Fisher plot fails. In Fig. 9b, the lines connecting data at the same  $\beta$  and lattice size differ significantly from straight lines.

We have found another difference between the behavior of the model close to the chiral phase transition around the point E and at smaller  $\beta$ . The scalar boson mass  $am_s$  gets small in the vicinity of E, whereas it remains of the order of cutoff or larger at the chiral transition for smaller  $\beta$ . In Fig. 10, both boson masses  $am_s$  and  $am_v$  are shown at  $\beta = 0.55$  and  $\beta = 0.64$  for  $am_0 = 0.04$ . A dip in  $am_s$  at  $\beta = 0.64$  around  $K = 0.315$  is clearly seen. It gets deeper when the lattice size is increased. Similar dips have also been found for other values of  $am_0$  and lattice sizes for various  $\beta'_E$ , whereas at  $\beta = 0.55$  or smaller the mass  $am_s$  does not decrease below 1 neither on small lattices nor on large ones. This difference, obvious in the quenched case, is thus present also with dynamical fermions. If a new correlation length diverges at some critical point and not at other ones, the most natural

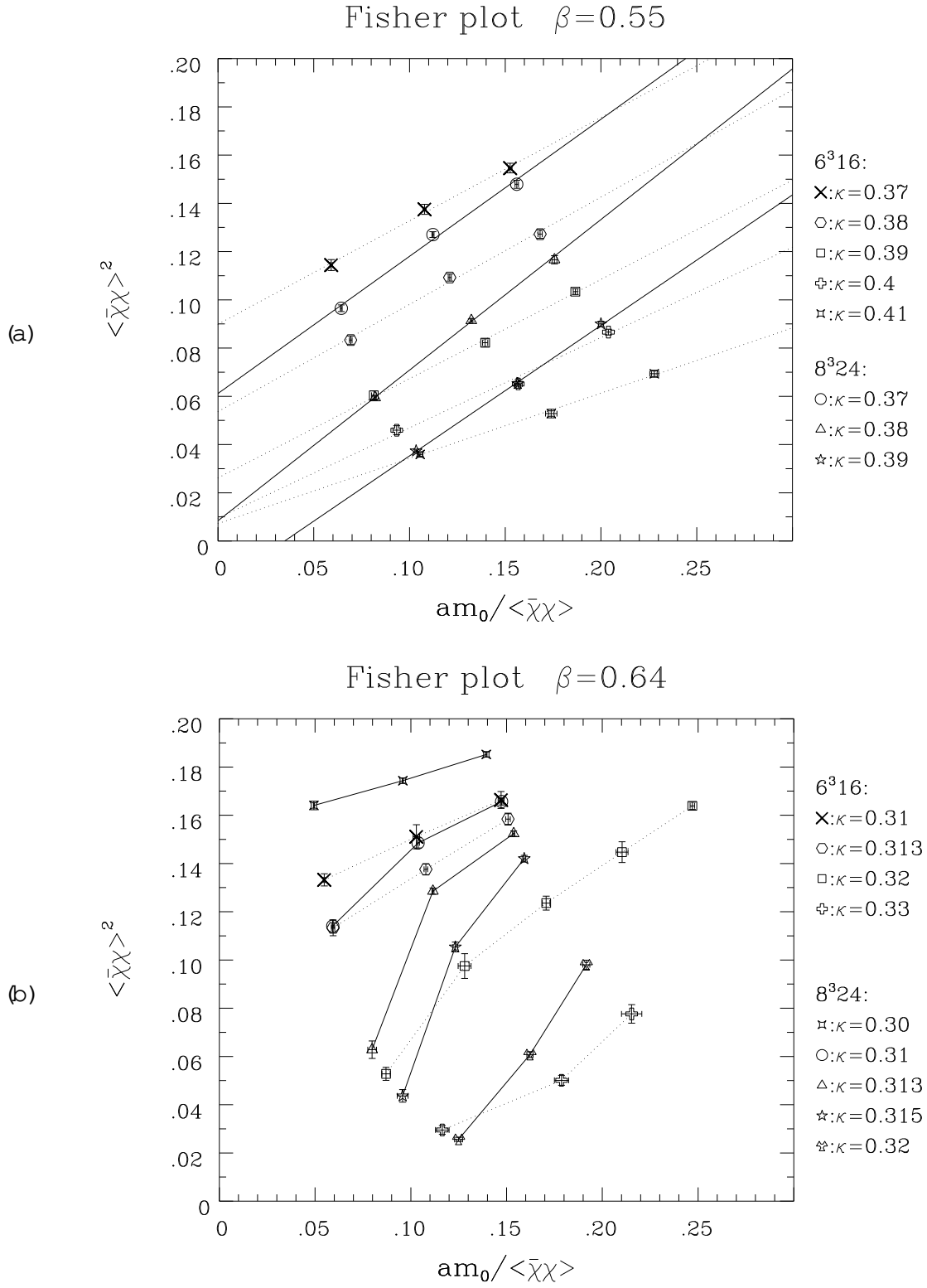


Figure 9:  $\langle \bar{\chi}\chi \rangle^2$  as a function of  $am_0/\langle \bar{\chi}\chi \rangle$  for fixed coupling parameters and lattice size (Fisher plots) at (a)  $\beta = 0.55$  and (b)  $\beta = 0.64$ . The straight lines in (a) indicate according to eq. (4.4) a mean field behavior.

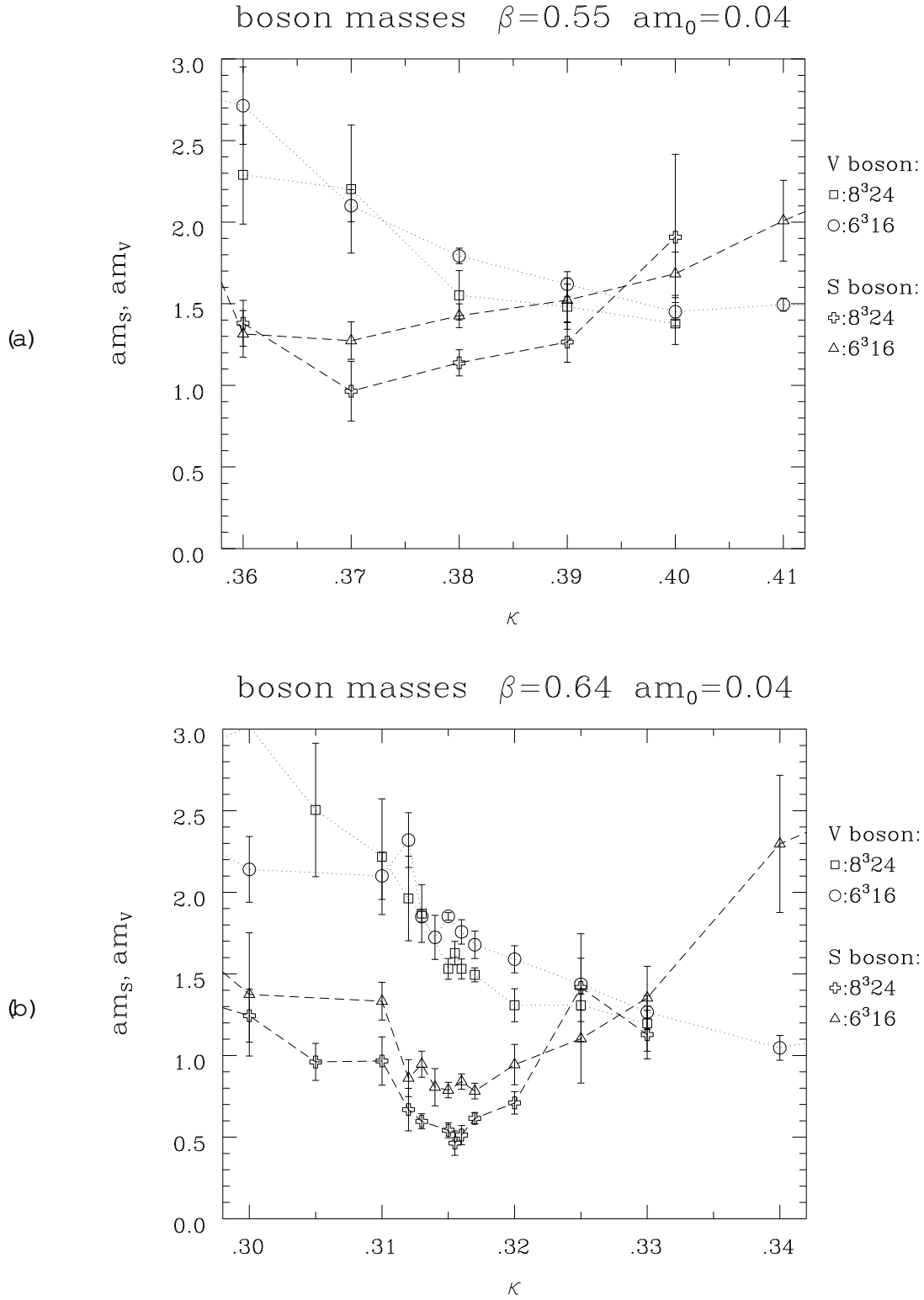


Figure 10: Vector and scalar boson masses,  $am_V$  and  $am_S$ , as functions of  $\kappa$  at (a)  $\beta = 0.55$  and (b)  $\beta = 0.64$ . To estimate the finite size effects two different lattice sizes ( $6^3 16$  and  $8^3 24$ ) are shown.



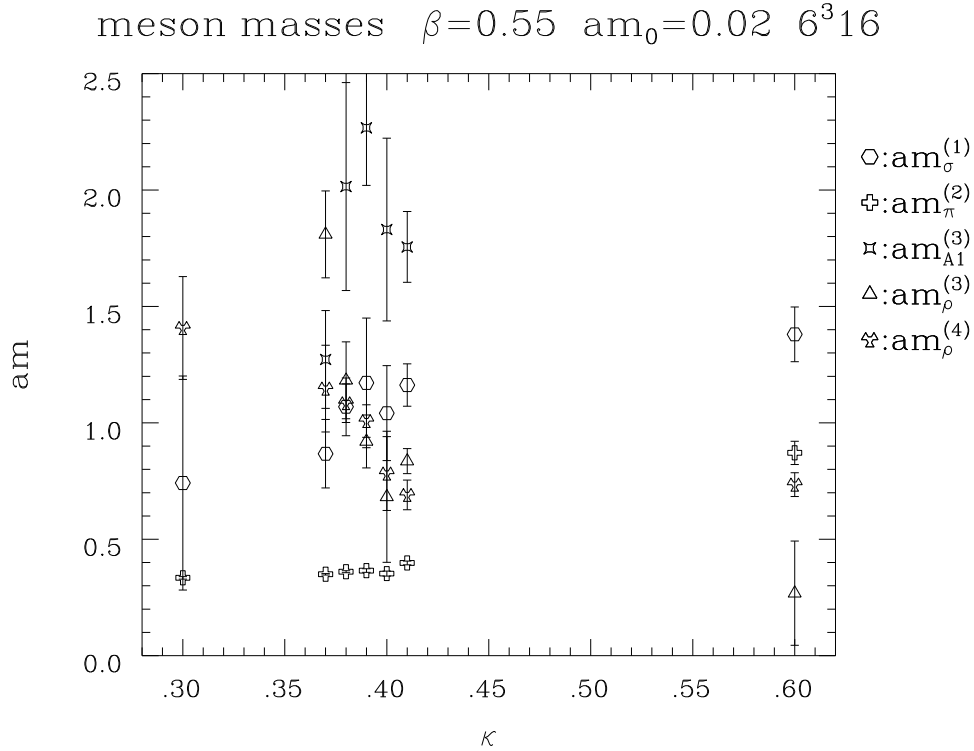


Figure 11: Meson states observable in the vicinity of the chiral phase transition. The states are denoted according to ref. [29].

explanation is that the scaling behavior is different.

These observations indicate that the scaling behavior in the vicinity of the point E is different from that at smaller  $\beta$ . This tentative conclusion is supported by the experience with tricritical points in various statistical mechanics models [31]. The tricritical exponents have usually quite different values from those describing the universality class of the adjacent critical manifolds. We also note that the chiral and magnetic phase transitions, occurring in the  $U_4$  model at small and large  $\beta$ , respectively, meet at the point E. Thus phenomena quite different from those known in both limit cases might occur here.

## 6 Summary and outlook

From the study of the behavior of several observables in the vicinity of the point E, as well as from some more general considerations about tricritical points, we conclude that the tricritical point E in the phase diagram of the  $U_4$  model is an interesting candidate for an investigation of the continuum limit of this model. The significant differences from the NJL-type model suggest that a continuum theory with massive fermions might arise which does not belong to the universality class of the Yukawa models in the sense of ref. [21].

To test this conjecture a laborious investigation of the scaling behavior of the model around the tricritical point E will be necessary, taking more observables into account. A rich spectrum is expected in the Nambu phase of the model, qualitatively similar to that one would guess in the case of QCD with one fermionic and one scalar quark (this analogy has been discussed in ref. [5]). Some glimpse at the states not too difficult to find is provided by figs. 10 and 11. In fig. 11 we show some meson masses. It has been checked in [12] that for the Goldstone boson mass  $am$  the relationship  $am \propto \sqrt{P \over am_0}$ , expected in the Nambu phase, holds. In this figure one can identify also states which are analogies of the  $\rho$ ,  $\pi$  and

$A_1$  mesons in QCD. Such states might accompany the massive fermion  $F$  and the scalar  $S$  also in the continuum limit of the  $U_4$  model constructed at the tricritical point  $E$ . If so, the spectrum would be rather different from that of the Yukawa models, supporting the conjecture of a new universality class.

## Acknowledgements

We thank V. Azcoiti, M. Gockeler, R. Horsley, M. Lindner, G. Schierholz and R.E. Shrock for discussions. We are grateful to the authors of ref. [20] for many explanations and H.A. Kastrup for continuous support. Most computations have been performed on Cray YMP/864 at HLRZ Jülich ( $6^3 16$  lattice) and VPP 500/4 Landesrechner in Aachen ( $8^3 24$  lattice).

## Microcanonical fermionic average method extended to eld theories with scalars

To perform the calculation of  $\chi^2$ , eq. (2.11), in the chiral limit the microcanonical fermionic average method developed for the gauge-fermion systems [22,23] has been extended to the fermion-gauge-scalar models [24]. Here we just outline the strategy.

The essential idea of the algorithm is the computation of the full effective action

$$S_e(E; m_0; N_f; \beta; \gamma) = -\ln M(E; \beta, \gamma) - 6V E + S_e^F(E; m_0; N_f; \beta, \gamma) \quad (A.1)$$

as a function of the pure gauge energy  $E$  and other bare parameters like  $m_0$ ,  $N_f$ ,  $\beta$  and  $\gamma$ , where

$$M(E; \beta, \gamma) = \int [dU] [d\psi] [d\bar{\psi}] \mathbb{E}_P(U) e^{-E} \exp[8V E_L(U; \beta, \gamma)] \quad (A.2)$$

is the density of states and

$$\begin{aligned} S_e^F(E; m_0; N_f; \beta, \gamma) &= -\ln \int [d\psi] [d\bar{\psi}] \det(U)^{\frac{N_f}{4}} e^{-E} \\ &= -\ln \frac{\int [dU] [d\psi] [d\bar{\psi}] \mathbb{E}_P(U) e^{-E} \det(U)^{\frac{N_f}{4}} \exp[8V E_L(U; \beta, \gamma)]}{M(E; \beta, \gamma)} \end{aligned} \quad (A.3)$$

is the effective fermionic action.  $M(E; \beta, \gamma)$  in (A.2) can be easily computed by quenched simulation. The main effort to be paid is to calculate  $S_e^F(E; m_0; N_f; \beta, \gamma)$  through (A.3) by means of microcanonical and Monte Carlo simulations [24]. For  $N_f = 4$ ,  $\langle \det(U) \rangle_E$  is the fermionic determinant averaged over the configurations with the probability distribution

$$\frac{\mathbb{E}_P(U) e^{-E} \exp[8V E_L(U; \beta, \gamma)]}{M(E; \beta, \gamma)}; \quad (A.4)$$

From (A.3), one sees that the effective fermionic action  $S_e^F$  does not depend on  $\beta$  and its dependence on  $m_0$  and  $N_f$  can be easily obtained, once the eigenvalues of the massless fermionic matrix for the decorrelated configurations at fixed  $E$  have been calculated by the Lanczos algorithm. Once  $S_e(E; m_0; N_f; \beta; \gamma)$  is known, the thermodynamical quantities such as  $\langle H_P \rangle$ ,  $\langle H_L \rangle$ ,  $\langle h \rangle$  and  $\chi^2$  can be obtained by deriving the partition function

$$Z = \int dE \exp[-S_e(E; m_0; N_f; \beta; \gamma)]; \quad (A.5)$$

or by saddle point analysis [24].

In [24], on  $6^4$  lattice and at finite  $m_0$ , comparisons with the results from the Hybrid Monte Carlo (HMC) method for a fermion-gauge-scalar model were made, and the HMC data were well reproduced. The advantage of the algorithm, in addition to its lower computational costs in searching the parameter space ( $m_0$ ;  $\beta$ ) compared to the conventional algorithms, is the accessibility of the chiral limit. Therefore the algorithm is very suitable for the phase structure analysis.

While having demonstrated the advantages of the algorithm on the  $6^4$  lattice, we would like to mention some open questions. For large lattice volumes, it is time and memory consuming to diagonalize the fermionic matrix. For example, on the  $8^4$  lattice, the amount of data required grows so fast that the algorithm has not been well tested. Although the Lanczos algorithm is parallelizable [23], it is not easily vectorizable. It is also not easy to evaluate observables other than the thermodynamical quantities. These problems are under further investigation.

## References

- [1] K.-I. Kondo, M. Tanabashi and K. Yamawaki, in T. Muta and K. Yamawaki, eds., *Proceedings of the Workshop on Dynamical Symmetry Breaking*, Nagoya (Nagoya University, 1990).
- [2] K. Cahill, *Phys. Lett.* 269B (1991) 129.
- [3] D. E. C lauge and G. G. Ross, *Nucl. Phys. B* 364 (1991) 43.
- [4] W. Bock, A. K. De, C. Frick, J. Jersak and T. Trappenberg, *Nucl. Phys. B* 378 (1992) 652.
- [5] C. Frick and J. Jersak, *Dynamical fermion mass generation by strong gauge interaction shielded by a scalar field*, preprint HLRZ 52/94, to be published in *Phys. Rev. D* vol. 51 (June 1995).
- [6] I.-H. Lee and R. E. Shrock, *Phys. Rev. Lett.* 59 (1987) 14.
- [7] I.-H. Lee and R. E. Shrock, *Nucl. Phys. B* 290 [FS20] (1987) 275.
- [8] I.-H. Lee and R. E. Shrock, *Nucl. Phys. B* 305 [FS23] (1988) 286.
- [9] R. E. Shrock, *Nucl. Phys. B (Proc. Suppl.)* 9 (1989) 77.
- [10] E. Dagotto and J. Kogut, *Phys. Lett.* 208B (1988) 475.
- [11] C. Frick and J. Jersak, *Nucl. Phys. B (Proc. Suppl.)* 42 (1995) 612.
- [12] X. Q. Luo and W. Franzki, *Nucl. Phys. B (Proc. Suppl.)* 42 (1995) 633.
- [13] W. Franzki and X. Q. Luo, *Nucl. Phys. B (Proc. Suppl.)* 42 (1995) 609.
- [14] I.-H. Lee and J. Shigemitsu, *Phys. Lett.* 169B (1986) 392.
- [15] A. K. De and J. Shigemitsu, *Nucl. Phys. B* 307 (1988) 376.
- [16] S. Aoki, I.-H. Lee and R. E. Shrock, *Phys. Lett.* 207B (1988) 471.

- [17] J. Kuti, Nucl. Phys. B (Proc. Suppl.) 9 (1989) 55.
- [18] C. Davies, S. Meyer and B. Pendleton, in Z. Horvath, L. Palla and A. Patkos, eds., *Frontiers of Nonperturbative Field Theory*, p. 106, Eger Theor. Workshop 1988 (World Scientific, Singapore, 1989).
- [19] S. Meyer and B. Pendleton, Phys. Lett. 253B (1991) 205.
- [20] A. Ali Khan, M. Gockeler, R. Horsley, P. E. L. Rakow, G. Schierholz and H. Stuben, Phys. Rev. D 51 (1995) 3751.
- [21] A. Hasenfratz, P. Hasenfratz, K. Jansen, J. Kuti and Y. Shen, Nucl. Phys. B 365 (1991) 79.
- [22] V. Azcoiti, G. Di Carlo and A. Grippo, Phys. Rev. Lett. 65 (1990) 2239.
- [23] V. Azcoiti, V. Laliena, X. Q. Luo, C. E. Piedra ta, G. D. A. Galante, A. F. Grippo, L. A. Fernandez and A. Vladikas, Phys. Rev. D 48 (1993) 402.
- [24] X. Q. Luo, Efficient Algorithm for Computer Simulations of the Fermion-Scalar Systems, preprint HLRZ 21/95.
- [25] K. Jansen, J. Jersak, C. B. Lang, T. Neuhaus and G. Vones, Nucl. Phys. B 265 [FS15] (1986) 129.
- [26] H. G. Evertz, K. Jansen, J. Jersak, C. B. Lang and T. Neuhaus, Nucl. Phys. B 285 [FS19] (1987) 590.
- [27] D. Callaway and R. Petronzio, Nucl. Phys. B 280 [FS18] (1987) 481.
- [28] J. L. Alonso et al., Phys. Lett. 296B (1992) 154; Nucl. Phys. B 405 (1993) 574.
- [29] M. F. L. Goltermann and J. Smit, Nucl. Phys. B 245 (1984) 61.
- [30] C. van den Doel and J. Smit, Nucl. Phys. B 228 (1983) 122.
- [31] I. D. Lawrie and S. Sarbach, in C. Domb and J. L. Lebowitz, eds., *Phase transitions and critical phenomena*, vol. 9, p. 1 (Acad. Press, New York, 1984).